Supplement of Atmos. Chem. Phys., 25, 11703–11718, 2025
https://doi.org/10.5194/acp-25-11703-2025-supplement

Atmospheric Chemistry and Physics
Open Access
EGU

Supplement of

Fertilization-driven pulses of atmospheric nitrogen dioxide complicate air pollution in early spring over the North China Plain

Tian Feng et al.

Correspondence to: Guohui Li (ligh@ieecas.cn)

Text S1. Definition of pollution accumulation index (PAI)

Boundary layer height (BLH) and wind speed (WS) are crucial meteorological fields for the occurrence of air pollutions, reflecting the atmospheric circulation conditions directly (Huang et al., 2017; Korshover and Angell, 2000; Su et al., 2018). Here, a pollution accumulation index (PAI) is defined using BLH (km) and WS (m s^{-1}) to represent the atmospheric dispersion capacity. The formula is as follows:

$$PAI = \frac{1}{BLH} \times \frac{1}{e^{WS}} \tag{4}$$

where PAI is dimensionless. The higher (lower) the PAI is, the poorer (better) the ventilation is and the more (less) the pollutants accumulate. The data are freely from the ERA5 products by the European Centre for Medium-Range Weather Forecasts. A higher PAI generally indicates meteorology being more favorable for pollution accumulation.

Text S2. Evaluation indices for simulation *vs.* observation

Four statistical indices, including mean bias (MB), normalized mean bias (NMB), root mean square error (RMSE), and index of agreement (IOA), are used to evaluate the model performance on mass concentrations of surface pollutants (Feng et al., 2021; Willmott, 1981):

$$IOA = 1 - \frac{\sum_{i=1}^{N}(S_i - O_i)^2}{\sum_{i=1}^{N}(|S_i - \bar{O}| + |O_i - \bar{O}|)^2} \tag{5}$$

$$MB = \frac{1}{N}\sum_{i=1}^{N}(S_i - O_i) \tag{6}$$

$$NMB = \frac{\sum_{i=1}^{N}(S_i - O_i)}{\sum_{i=1}^{N} O_i} \times 100\% \tag{7}$$

$$RMSE = \left[\frac{1}{N}\sum_{i=1}^{N}(S_i - O_i)^2\right]^{\frac{1}{2}} \tag{8}$$

where S_i and O_i are the simulated and observed variables, respectively. N is the total number of simulation variables, and $\bar{O}$ denotes the average of observations. The IOA varies in the range from 0 to 1, and higher values suggest better agreement between the simulation and the observation.

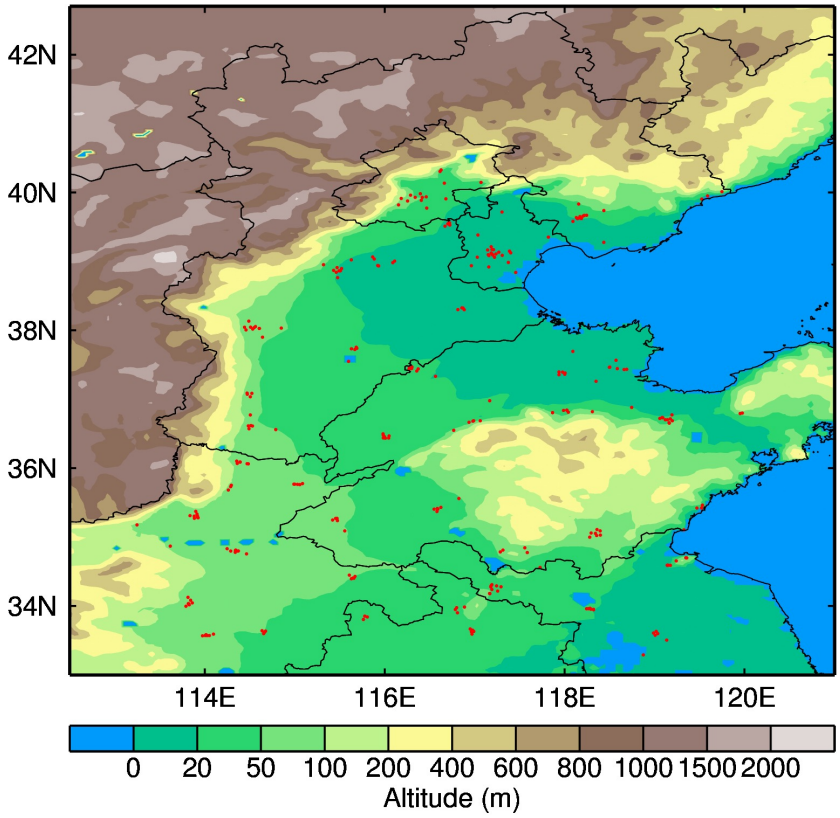

Figure S1. Map showing the locations of the 141 monitoring stations for air quality (red dots) over the NCP. Data are from the CNEMC. The color shading represents the topography of this region, with water areas depicted in blue.

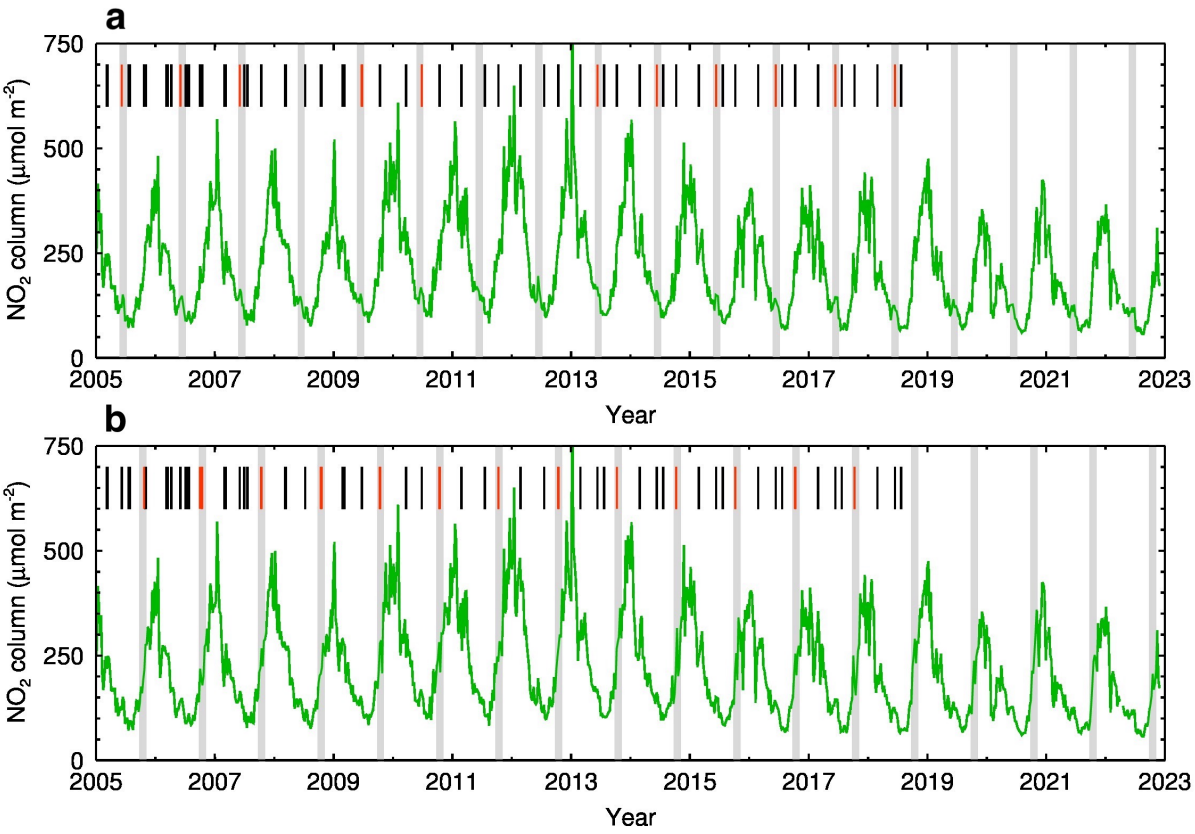

Figure S2. A re-presentation of the long-term tropospheric NO_2 column time series shown in Figure 2a, but with (a) June and (b) October pulses highlighted using grey bars. The red bars show the fertilization events during sowing periods for maize and winter wheat in (a) June and (b) October, respectively.

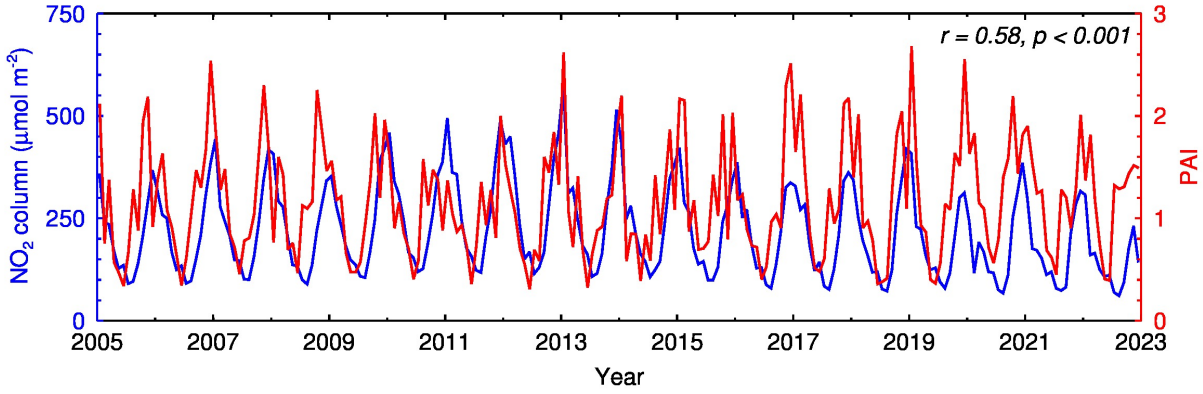

Figure S3. Linkage between NO_2 column over the NCP from 2005 to 2022 and PAI. Long-term (2005-2022) monthly NO_2 column is generally connected to the PAI ($r = 0.58$, confidence level exceeding 99.9%) over the NCP, but there are noticeable discrepancies in the timings of the sub-peaks between them.

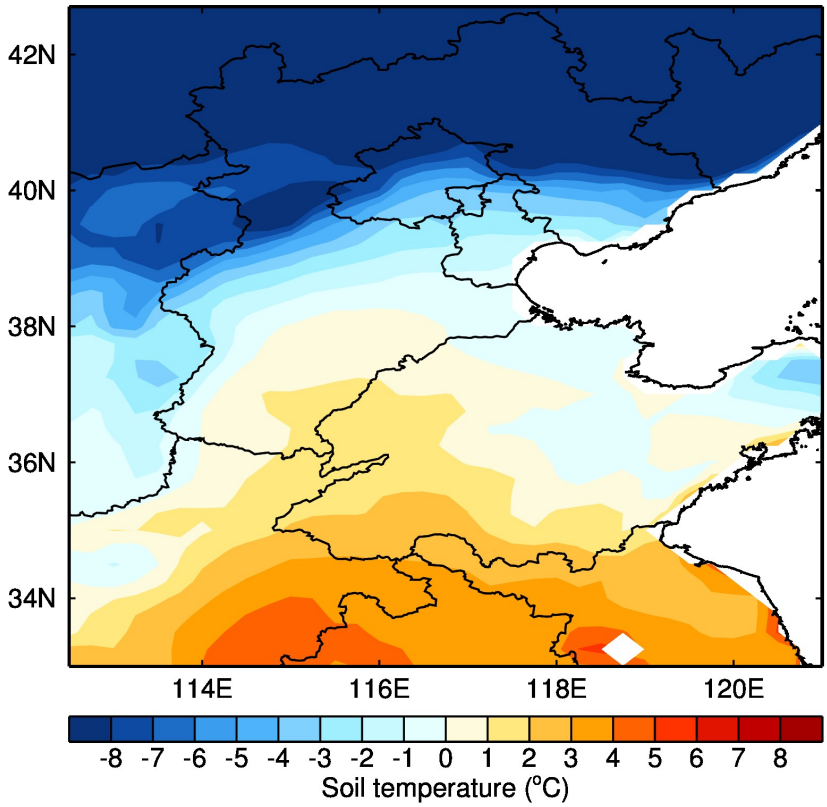

Figure S4. Spatial distribution of the minimum daily soil temperature of the top layer over the NCP during the period from 20 February to 31 March, 2020. Data are from the ERA5 reanalysis. The white areas show waters.

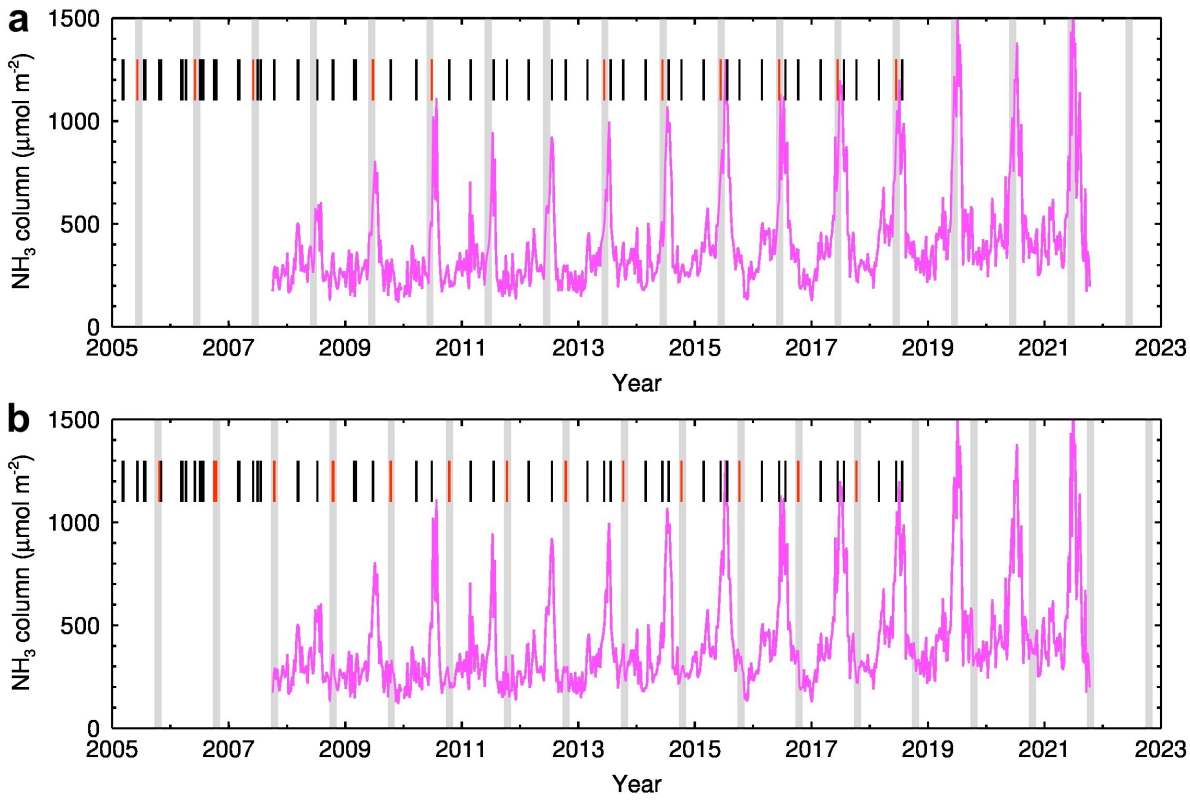

Figure S5. Other sub-peaks of NH_3 column over the NCP from 2007 to 2022. (a and b) Satellite-retrieved other pulses of NH_3 column in June and October, respectively. Intersections of the gray bars and the green lines, and the short bars are similar to those in Figure S4.

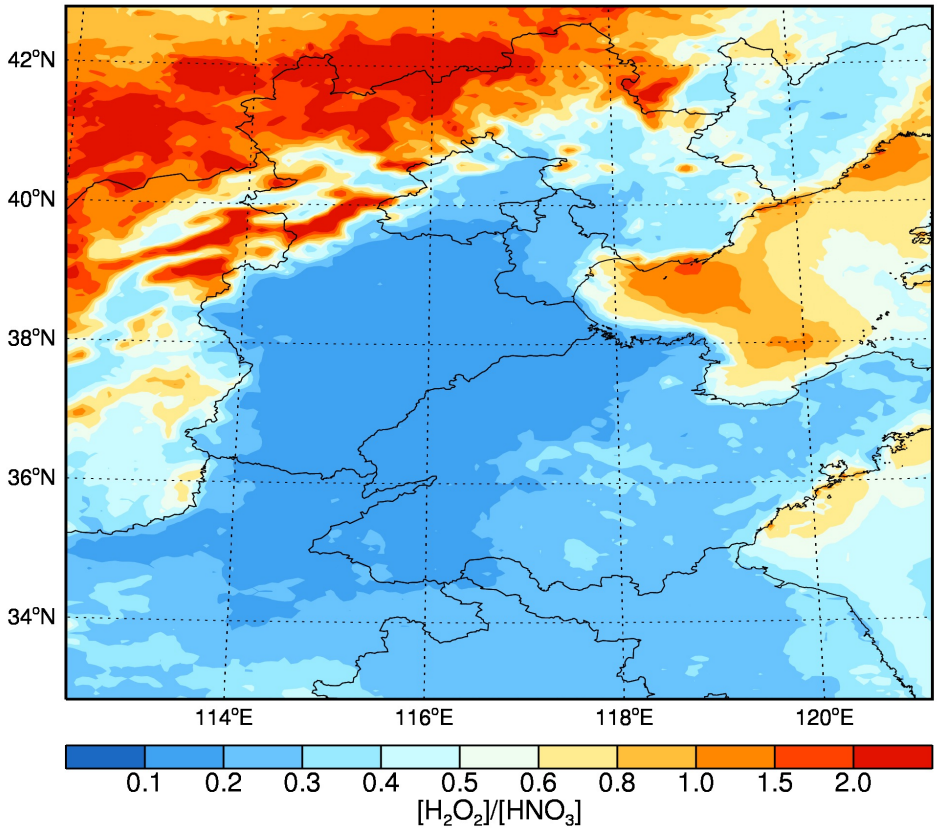

Figure S6. Spatial distribution of O_3 formation sensitivity to precursors indicated by the $[H_2O_2]/[HNO_3]$ ratio in March 2020 over the NCP. A ratio less than 0.3, great than 0.5, and between 0.3 and 0.5 indicates the O_3 formation under VOC-sensitive, NO_x-sensitive and transition regimes, respectively.

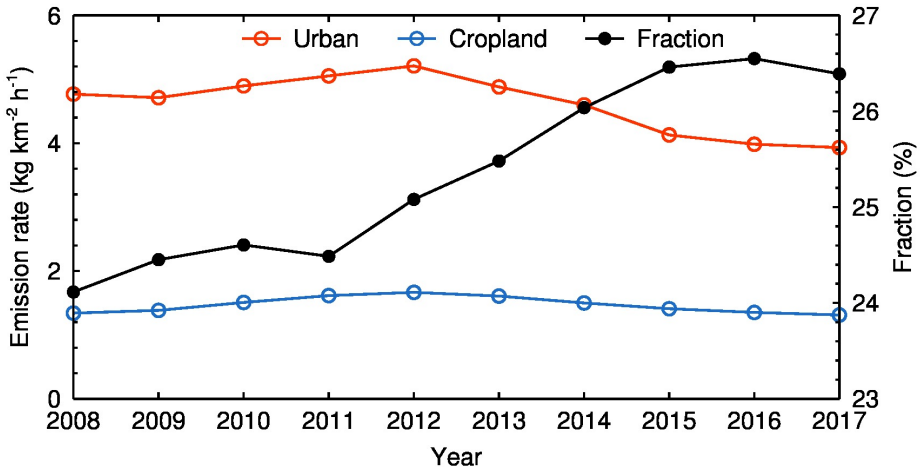

Figure S7. Temporal variations of annual anthropogenic NOx emission rate averaged over urban areas (red) and croplands (blue), respectively, in the NCP and the fraction of the emission over croplands in the total (black) during 2008-2017. The data are derived from the MEIC v1.3 emission inventory.

References

Feng, T., Zhao, S., Hu, B., Bei, N., Zhang, X., Wu, J., Li, X., Liu, L., Wang, R., Tie, X. and Li, G.: Assessment of Atmospheric Oxidizing Capacity Over the Beijing-Tianjin-Hebei (BTH) Area, China, J. Geophys. Res. Atmos., 126(7), e2020JD033834, doi:10.1029/2020JD033834, 2021.

Huang, Q., Cai, X., Song, Y. and Zhu, T.: Air stagnation in China (1985-2014): Climatological mean features and trends, Atmos. Chem. Phys., 17(12), 7793–7805, doi:10.5194/acp-17-7793-2017, 2017.

Korshover, J. and Angell, J. K.: A Review of Air-Stagnation Cases in the Eastern United States During 1981 - Annual Summary, Mon. Weather Rev., 110(10), 1515–1518, doi:10.1175/1520-0493(1982)110<1515:AROASC>2.0.CO;2, 2000.

Su, T., Li, Z. and Kahn, R.: Relationships between the planetary boundary layer height and surface pollutants derived from lidar observations over China: regional pattern and influencing factors, Atmos. Chem. Phys., 18(21), 15921–15935, doi:10.5194/acp-18-15921-2018, 2018.

Willmott, C. J.: On the Validation of Models, Physical Geography, 2(2), 184–194, doi:10.1080/02723646.1981.10642213, 1981.